Research Report

2004-04T

Closed-Form Analysis of Adjustable Speed Drive Performance Under Input Voltage Unbalance and Sag Conditions

K. Lee, W.E. Berkopec, T.M. Jahns*, T.A. Lipo*

Eaton Electrical
4201 N. 27th St.
Milwaukee, WI 53216

*University of Wisconsin, Madison
1415 Engineering Dr.
Madison, WI 53706

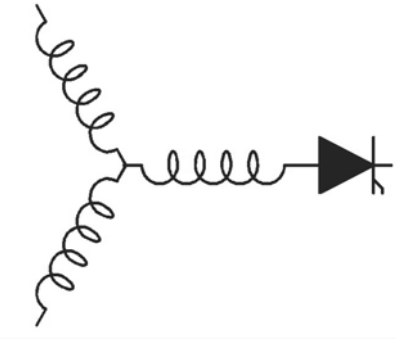

Wisconsin
Electric
Machines &
Power
Electronics
Consortium

University of Wisconsin-Madison
College of Engineering
Wisconsin Power Electronics Research Center
2559D Engineering Hall
1415 Engineering Drive
Madison WI 53706-1691

© 2004 Confidential

Closed-Form Analysis of Adjustable-Speed Drive Performance Under Input-Voltage Unbalance and Sag Conditions

Kevin Lee, *Senior Member, IEEE*, Thomas M. Jahns, *Fellow, IEEE*, William E. Berkopec, and Thomas A. Lipo, *Life Fellow, IEEE*

***Abstract*—Voltage unbalance or sag conditions generated by the line excitation can cause the input rectifier stage of an adjustable-speed drive (ASD) to enter single-phase rectifier operation. This degradation of the input power quality can have a significant negative impact on the induction-machine performance characteristics. This paper provides an approximate closed-form analysis of the impact of line-voltage sags and unbalance on the induction-machine phase voltages, currents, and torque pulsations for a general-purpose ASD consisting of a three-phase diode bridge rectifier, a dc link, and a pulsewidth modulation (PWM) inverter delivering constant volts-per-hertz excitation. Attention is focused on the impact of the dominant second harmonic of the line frequency, which appears in the dc link voltage during the sag/unbalance conditions, neglecting the impact of the other higher order harmonics. In addition to the closed-form analytical results that assume constant rotor speed, both simulation and experimental results are presented, which confirm the key analytical results, including the dominance of the second harmonic in the resulting torque pulsations. The analytical results can be used as a valuable design tool to rapidly evaluate the approximate impact of unbalance/sag conditions on ASD machine performance.**

***Index Terms*—Adjustable-speed drives (ASDs), input-voltage sag and unbalance, power quality, torque pulsation.**

I. Introduction

THE NATURE of power-quality problems, their frequency, and the problems they cause have been reported in [1]–[3]. Input-voltage unbalance, sags, waveform distortion, frequency variation, noise, spikes, outages, and surges are all well-known power-quality disturbances. Fig. 1 illustrates the approximate percentage voltage unbalance found on power distribution systems in the United States based on data extracted from field survey results [4].

Adjustable-speed drives (ASDs) are widely used in both industrial and commercial applications as the most versatile and efficient means of achieving motion control. Input-voltage unbalance and sag conditions can have serious performance consequences in ASDs, including abnormally low input line power factor, high input-current harmonic distortion, overstressed dc-bus capacitors, high pulsating torque, and motor overheating. In the U.S. today, the overall cost of motor loss of life due to harmonic pollution and voltage imbalance is estimated to be U.S. $1–$2 billion per year [5].

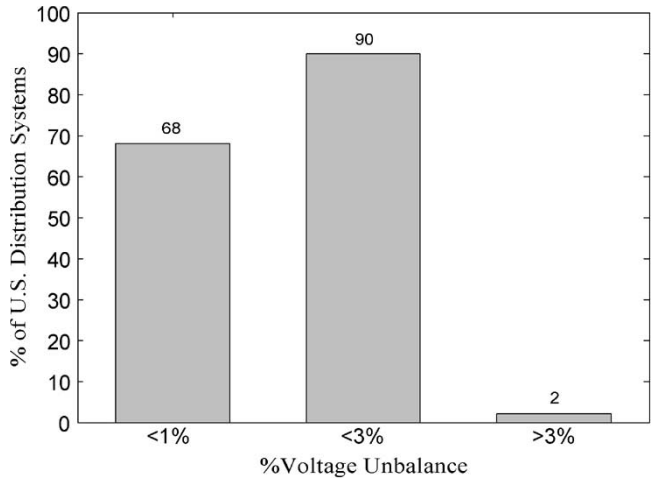

Fig. 1. Approximate voltage-unbalance percentage in U.S. distribution systems [4].

In previous studies, considerable attention has been given to calculating sixth-harmonic torque pulsations caused by balanced three-phase nonsinusoidal excitation. This type of pulsating torque [6] is principally produced by interactions between the fundamental electromagnetic flux and the fifth and seventh harmonic currents. A method of predicting the sixth-harmonic electromagnetic torque of an induction motor caused by excitation with six-step voltage waveforms was presented in [7]. The resulting pulsating torque can have undesirable effects [8] including vibration and audible noise [9], [10]. For example, pulsating torque can excite the natural frequencies of the mechanical drivetrain, degrading system performance [11], [12].

The attention in this paper is focused on the effects of unbalanced input line excitation of general-purpose ASDs that consist of a three-phase rectifier input stage, a dc link, and a pulsewidth modulation (PWM) inverter stage that delivers constant volts-per-hertz excitation. Although dc bus inductors can be installed to improve the inverter output quality, their use is not common in ASDs sold today because of their size and cost. As a result, the ASD model adopted for this paper uses only capacitance on the dc link.

Paper IPCSD-05-111, presented at the 2004 IEEE Power Electronics Specialist Conference, Aachen, Germany, June 20–26, and approved for publication in the IEEE TRANSACTIONS ON INDUSTRY APPLICATIONS by the Industrial Drives Committee of the IEEE Industry Applications Society. Manuscript submitted for review November 15, 2005 and released for publication January 10, 2006.

K. Lee and W. E. Berkopec are with Eaton Electrical, Milwaukee, WI 53216 USA (e-mail: KevinLee@eaton.com; WilliamEBerkopec@eaton.com).

T. M. Jahns and T. A. Lipo are with University of Wisconsin, Madison, WI 53706 USA (e-mail: jahns@engr.wisc.edu; lipo@engr.wisc.edu).

Digital Object Identifier 10.1109/TIA.2006.872953

0093-9994/$20.00 © 2006 IEEE

Transient voltage sags or steady-state voltage-unbalance conditions in the three-phase input line voltages can cause the rectifier stage to transition into single-phase rectifier operation. Such operation creates significant amounts of harmonic voltage on the dc link at twice the line frequency (120 Hz for 60-Hz excitation). This link-voltage ripple at the inverter input terminals affects the PWM output voltage waveforms, causing low-frequency harmonic currents to flow in the machine. These harmonic machine currents, in turn, create undesired torque pulsations (i.e., ripple torque) that are dominated by the second harmonic of the input line frequency (120 Hz), the same frequency that appears in the dc link voltage.

The new contribution of this paper is the development of closed-form expressions that approximately capture the relationship between the input-voltage unbalance/sag conditions and the resulting induction-machine performance characteristics for finite values of input line inductance and dc bus capacitance. The attention is focused on the calculation of induction-machine harmonic current and pulsating-torque amplitudes in response to the second line-harmonic frequency component that appears in the dc link voltage. The results of this investigation are valuable since the second line harmonic that appears in the dc link voltage dominates the resulting harmonic effects.

The closed-form analytical expressions are verified using a combination of dynamic simulations and experimental tests. A 3.7-kW 460-V ASD system is used as the target for these verification efforts, providing valuable results that raise confidence in the accuracy and value of the analytical results. The availability of these relationships provides a convenient tool for rapidly and quantitatively evaluating the impact of varying levels of input line-voltage sag and unbalance on the ASD induction-machine performance.

II. System Description

The most common types of voltage sags experienced by three-phase loads have been classified as types A, C, and D [1]. For a type-A voltage sag, all three phase voltages drop in magnitude by the same amount while retaining 120° displacements. For type C or D sags, the three phase voltages change by different amounts and their phase angles change as well, creating unbalanced excitation conditions.

In this paper, a type-C sag and its associated voltage unbalance was selected as the target input excitation condition for study. The type-C sag was chosen because it is relatively common among voltage-sag events and causes the rectifier to transition into single-phase conduction quite easily. Fig. 2 shows a voltage phasor diagram of a typical type-C sag condition. As noted above, both the amplitudes and the phase angles of the phase B and C voltages change from their balanced excitation values during a type-C sag.

For the ASD configurations that are the subject of this investigation, three-phase ac line voltages are fed to a three-phase rectifier (D_1–D_6) bridge, as shown in Fig. 3. The three-phase input line-impedance values are equal (i.e., balanced), consisting of line inductance L_a and resistance R_a. The dc bus voltage is buffered by dc bus capacitance C_d. The PWM

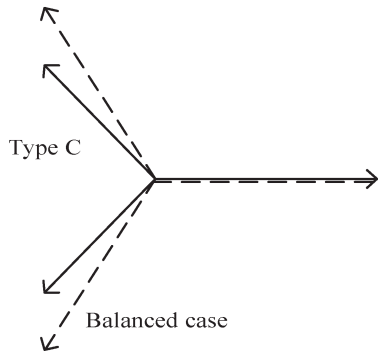

Fig. 2. Phasor diagram of type-C three-phase unbalanced input-voltage sag.

inverter consists of six insulated gate bipolar transistor (IGBT) switches (SW_1–SW_6) and their antiparallel diodes. PWM control of these switches is used to synthesize variable-frequency variable-amplitude ac-voltage waveforms that are delivered to the induction machine following a constant volts-per-hertz algorithm.

The input rectifier stage of the ASD can easily slip into single-phase operation during such sag/unbalance input excitation conditions. Fig. 4 provides an example of how the dc bus voltage and the input current waveforms change as a function of the input line inductance (L_a) values [14] for a type-C sag with 2.5% voltage unbalance.

The dominant ac component in the resulting bus voltage V_d waveform occurs at the second line-harmonic frequency (120 Hz). It is this second-harmonic voltage component that, in turn, dominates the generation of undesirable line sag/unbalance effects in the induction-machine operating characteristics. Attention is focused next on developing closed-form expressions that quantify the induction-machine performance effects caused by this second-harmonic component.

III. Analysis

A. DC-Bus Voltage Analysis

As discussed in the preceding section, the rectifier stage can enter the single-phase rectifier mode with discontinuous conduction. Assuming that the inverter load can be modeled as a fixed resistor R_L for a particular operating point, we define the dc-bus current (i_d) and voltage (V_d) as state variables in a second-order system. The system differential equations can be summarized during the rectifier conduction and nonconduction intervals, respectively, as

For $t_\mathrm{in} < t < t_\mathrm{ex}$

$$V_\mathrm{s} = i_\mathrm{d} \cdot R_\mathrm{s} + L_\mathrm{s}\frac{di_\mathrm{d}}{dt} + V_\mathrm{d} \tag{1}$$

$$i_\mathrm{d} = C_\mathrm{d} \cdot \frac{dV_\mathrm{d}}{dt} + \frac{V_\mathrm{d}}{R_\mathrm{L}} \tag{2}$$

and for $t_\mathrm{ex} < t < t_\mathrm{in} + \frac{1}{2} \cdot T$

$$i_\mathrm{d} = 0 \tag{3}$$

$$\frac{dV_\mathrm{d}}{dt} = -\frac{1}{C_\mathrm{d}R_\mathrm{L}}V_\mathrm{d} \tag{4}$$

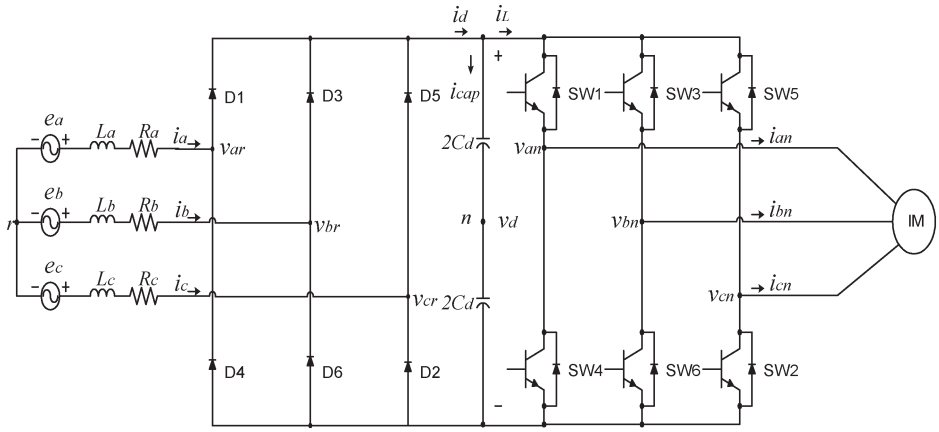

Fig. 3. Induction-machine ASD power circuit diagram including a three-phase input rectifier stage, a dc link, and a three-phase output inverter stage.

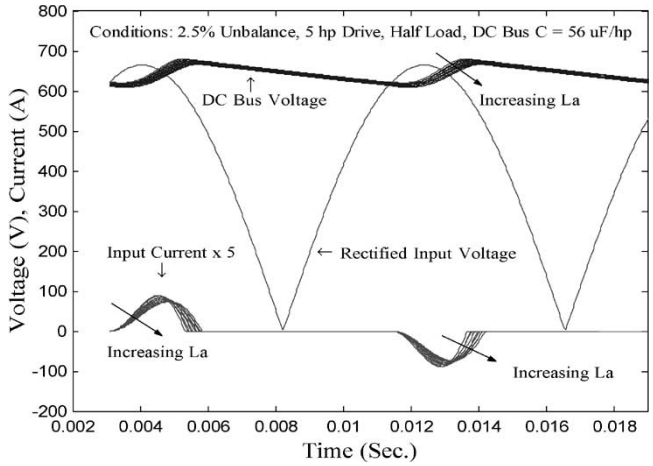

Fig. 4. Rectified input line voltage during single-phase operation caused by a type-C sag with 2.5% unbalance, showing dc-bus input current i_{dc} and dc-bus voltage v_{d} with varying line inductance (1%–2%).

where $L_{\mathrm{s}} = 2L_{\mathrm{a}}$, $R_{\mathrm{s}} = 2R_{\mathrm{a}}$, t_{in} is the bus current i_{d} inception time, t_{ex} is the extinction time, and T is the period of the ac excitation frequency (e.g., 1/60 = 16.7 ms for 60-Hz excitation) (see Fig. 4).

The closed-form solution of the dc-bus voltage $V_{\mathrm{d}}(t)$ is expressed as

$$V_{\mathrm{d}}(t) = \begin{cases} A \cdot e^{-\alpha t} \cdot \cos(\beta t) + B \cdot e^{\alpha t} \cdot \sin(\beta t) \\ \quad + M \cdot \cos(\omega t) + N \cdot \sin(\omega t), & t_{\mathrm{in}} < t < t_{\mathrm{ex}} \\ V_{\mathrm{d}}(t_{\mathrm{ex}}) \cdot e^{-\frac{t - t_{\mathrm{ex}}}{C_{\mathrm{dc}} R_{\mathrm{L}}}}, & t_{\mathrm{ex}} < t < t_{\mathrm{in}} + \frac{T}{2} \end{cases} \tag{5}$$

where the coefficient definitions and derivation details are provided in a separate paper [13].

This closed-form bus-voltage expression makes it possible to analyze the effects of finite values of input line inductance and dc bus-capacitance values on induction-machine performance during sag/unbalance conditions.

B. Induction-Machine Circuit Analysis

The voltage-source inverter (VSI) diagram in Fig. 5 is used to define key terminal-voltage variables in the ASD inverter

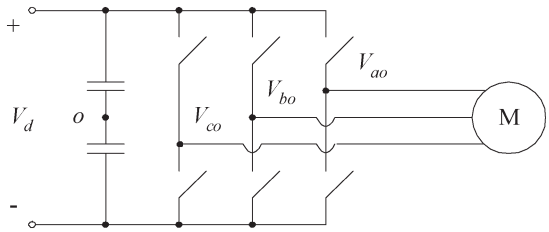

Fig. 5. Three-phase VSI diagram.

stage. For PWM operation, the output voltage waveforms of the inverter can be calculated by multiplying the dc bus voltage V_{d} with the inverter PWM switching function [14].

Under input-voltage unbalance or sag conditions, the presence of the second line frequency $(2\omega_{\mathrm{i}})$ harmonic voltage component in the dc bus voltage generates low-frequency harmonic components in the inverter output voltages at the sum and difference frequencies with the inverter output frequency (ω_0). For purposes of this analysis, it is assumed that the inverter PWM algorithm does not include any capability to detect and compensate for dc bus-voltage ripple.

Neglecting the impact of the higher order harmonic components in the dc bus voltage, the motor phase a line-to-midpoint voltage (V_{a0}) can be approximated as

$$V_{a0}(\omega_0 t) = \frac{1}{2} \cdot V_{\mathrm{d}}(t) \cdot B_1 \cdot \sin(\omega_0 t) \tag{6}$$

where ω_0 is the inverter output fundamental frequency and B_1 is the Fourier coefficient of the fundamental-frequency component of the inverter switching function [14] at ω_0.

It is apparent from the Fig. 4 waveforms that the dominant ac frequency component in the dc bus voltage under input-voltage sag and unbalance conditions appears at twice the input frequency $(2\omega_{\mathrm{i}})$. Thus, the dc bus voltage $V_{\mathrm{d}}(t)$ in (5) can be approximated as

$$V_{\mathrm{d}}(t) = V_{\mathrm{dc}} + V_{\mathrm{dc2}} \cdot \cos(2\omega_{\mathrm{i}} t + \theta_2) \tag{7}$$

where V_{dc} is the average value of the dc bus voltage, V_{dc2} is the amplitude of the second-harmonic voltage component, and θ_2

is the corresponding phase angle. Substituting (7) into (6), the phase voltage can be expressed approximately as

$$V_{a0}(\omega_0 t) = \frac{1}{2} \cdot V_{\rm dc} \cdot B_1 \sin(\omega_0 t) + \frac{1}{2} \cdot V_{\rm dc2} \cdot B_1 \cdot \cos(2\omega_{\rm i} t + \theta_2) \cdot \sin(\omega_0 t). \quad (8)$$

This phase-voltage expression can be restated by applying the following trigonometric identity

$$\cos A \cdot \sin B = \frac{1}{2} \cdot [\sin(A+B) - \sin(A-B)] \quad (9)$$

leading to

$$V_{a0}(\omega_0 t) = \frac{1}{2} \cdot V_{\rm dc} \cdot B_1 \cdot \sin(\omega_0 t) + \frac{1}{4} \cdot V_{\rm dc2} \cdot B_1 \cdot [\sin(2\omega_{\rm i} t + \omega_0 t + \theta_2) - \sin(2\omega_{\rm i} t - \omega_0 t + \theta_2)]. \quad (10)$$

This form of the phase-voltage expression provides valuable physical insight by showing that each phase voltage contains three major frequency components: a steady-state component at ω_0, a sum-frequency component at $2\omega_{\rm i} + \omega_0$, and a difference-frequency component at $2\omega_{\rm i} - \omega_0$. These latter two components are caused by the single-phase rectifier operation and are undesired.

The resulting machine phase currents will contain components at these same three frequencies. Provided that an assumption of constant rotor speed is made, closed-form solutions can be derived for the phase currents and the resulting machine torque under the unbalanced excitation conditions.

More specifically, the resulting phase a current will have the following form:

$$I_a(t) = I_{\rm s0} \cos(\omega_0 t + \phi_0) + I_{\rm s1} \cos((2\omega_{\rm i} + \omega_0)t + \phi_1) + I_{\rm s2} \cos((2\omega_{\rm i} - \omega_0)t + \phi_2) \quad (11)$$

while the instantaneous machine torque can be expressed as

$$T_{\rm e} = T_{\rm e0} + T_{\rm e2} \cos(2\omega_{\rm i} t + \phi_2) + T_{\rm e4} \cos(4\omega_{\rm i} t + \phi_4). \quad (12)$$

Details regarding the derivations of these current and torque expressions and the corresponding coefficients are provided in the Appendix. Significantly, the torque expression in (12) includes an average dc term that is contributed by the balanced three-phase excitation, and pulsating-torque components at twice and four times the line frequency that appear because of the input-voltage unbalance.

C. Closed-Form Analysis Results

The closed-form analysis described in the preceding section has been applied to compute the instantaneous stator-current and torque expressions for the 3.7-kW induction machine described in Section I. The parameters for this machine are provided in the Appendix.

Calculated waveforms are shown in Figs. 6 and 7 for a 460-V input line excitation with type-C sag conditions at 2.5% voltage unbalance. This input excitation causes a 17.4-$V_{\rm rms}$ voltage ripple at 120 Hz superimposed on the average dc bus voltage of 632 $V_{\rm dc}$. In this case, it is assumed that the inverter delivers rated voltage (460 V) to the machine at its rated frequency (ω_0) of 60 Hz with 50% rated load.

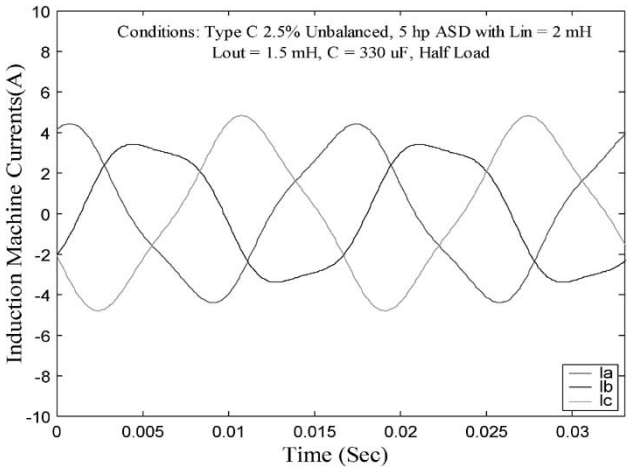

Fig. 6. Closed-form analysis results of machine phase currents during type-C sag with 2.5% voltage unbalance (50% load).

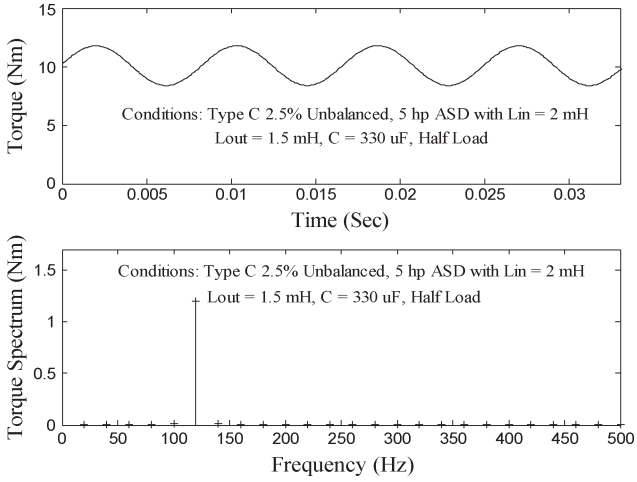

Fig. 7. Closed-form analysis results of machine-torque frequency spectrum during type-C sag with 2.5% voltage unbalance (50% load).

This particular operating condition of $\omega_0 = \omega_{\rm i} = 60$ Hz is an interesting case since the sum and difference frequencies $[(2\omega_{\rm i} + \omega_0)$ and $(2\omega_{\rm i} - \omega_0)]$ that appear in the machine stator currents occur at 180 Hz (positive-sequence third-harmonic component) and -60 Hz (negative-sequence fundamental component), respectively. This causes the unbalanced stator phase-current waveforms in Fig. 6.

Fig. 7 shows the induction-machine-torque waveform for this same operating condition along with its frequency spectrum. The upper plot of Fig. 7 shows an average torque of 10 N · m with pulsating torque that is dominated by the $2\omega_{\rm i}$ (120 Hz) component in (12). The lower plot in Fig. 7 shows the pulsating-torque frequency spectrum (in rms newton meter) that contains only the 120-Hz component. This is due to the fact that the higher order torque harmonics were not included in the closed-form analysis. The peak-to-peak torque pulsation at 120 Hz is 3.38 N · m, corresponding to 33.8% of the 10-N · m average torque at 50% rated load.

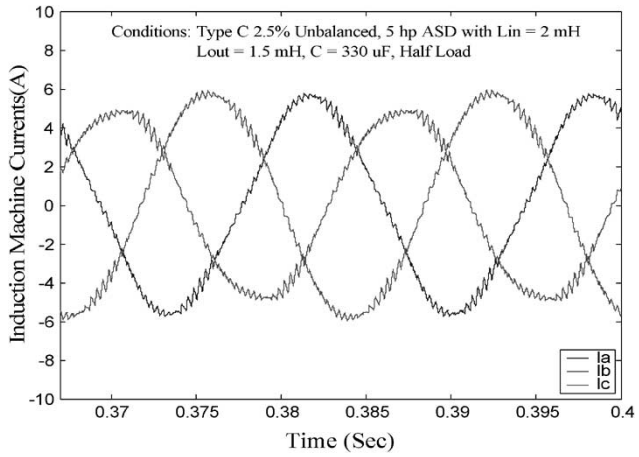

Fig. 8. Simulation results of machine phase currents during type-C sag with 2.5% voltage unbalance (50% load).

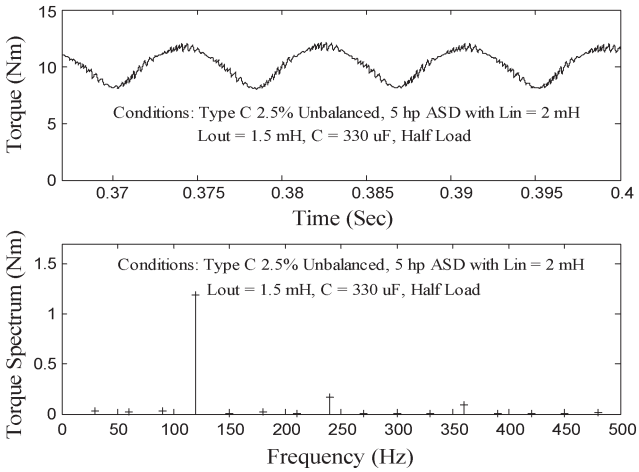

Fig. 9. Simulation results of machine-torque frequency spectrum during type-C sag with 2.5% voltage unbalance (50% load).

IV. Simulation Results

The drive system shown in Fig. 3 has been simulated using Simplorer to verify the analytical results presented above. This simulation includes explicit models of the diode rectifier stage and space-vector PWM operation of the inverter stage so that it captures the effects of higher order harmonics in the dc-bus voltage under input line sag/unbalance conditions (i.e., beyond second line harmonic) that are neglected in the closed-form analysis.

Figs. 8 and 9 show the induction-machine stator currents and torque for approximately the same operating conditions used to calculate the waveforms in Figs. 6 and 7. The simulated current waveforms match the major features of the calculated currents in Fig. 6 quite well, although the simulated current waveforms include the effects of the PWM switching frequency.

The upper plot of Fig. 9 shows the predicted torque waveform from the simulation that includes an average torque of 10 N · m to meet the 50% load, together with torque pulsations at 120 Hz and higher frequency harmonics. The lower plot in Fig. 9 shows the frequency spectrum of the torque waveform (in rms newton meter).

The pulsating torque in the simulated (Fig. 9) waveform is dominated by the second line-harmonic component as expected. However, the simulated torque waveform also includes small but nonzero Fourier components at higher order harmonics of the input line frequency, as well as the impact of the PWM switching frequency. The peak-to-peak amplitude of the simulated torque waveform is 3.36 N · m, matching the closed-form predicted value very closely.

The positive correspondence between the calculated and simulated current and torque waveforms helps to build confidence in the validity of the closed-form analysis.

V. Experimental Results

Experimental tests have been carried out using a 3.7-kW 460-V 60-Hz ASD mounted on a laboratory dynamometer. The test configuration is illustrated in Fig. 10, consisting of a programmable voltage-sag generator, a drive isolation transformer, the ASD under test, an induction machine, a load machine excited by a four-quadrant ASD, and a Labview-based computer system designed to provide data acquisition, monitoring, and control functions.

Figs. 11 and 12 show the measurement results of the test-machine stator currents for both balanced and unbalanced (type-C sag) input-voltage excitation conditions. The current waveforms in Fig. 12 for 2.5% unbalance with 50% load show many of the same features as the calculated and simulated current waveforms in Figs. 6 and 8, providing further confirmation of the closed-form analytical results.

An in-line torquemeter was used to measure the amplitude of the 120-Hz pulsating-torque component that was generated by the unbalance conditions. Special consultations were made with the torquemeter manufacturer to ensure that 120-Hz measurement could be made within the useful bandwidth of the instrument.

Table I provides an interesting comparison of the measured peak-to-peak pulsating-torque amplitude compared with the predicted values from the closed-form analysis and the simulation. The same test conditions of 50% rated load and type-C sag conditions with 2.5% voltage unbalance were applied in all three cases. The agreement between the pulsating-torque amplitude derived from the closed-form analysis, the simulation, and experimental tests is very good. Such comparisons provide evidence that the closed-form expressions presented in this paper can be applied to develop useful estimates of the impact of unbalanced excitation on induction-machine performance.

VI. Conclusion

This paper contributes to a better understanding of the effects of input line-voltage sag/unbalance conditions on the operation of adjustable-speed induction-machine drives by providing closed-form expressions to estimate the resulting machine stator-current and torque waveforms. The derivation of these expressions using dq complex equivalent circuit analysis techniques clearly shows how input line-voltage unbalance gives rise to dc-bus voltage ripple and torque pulsations that falls

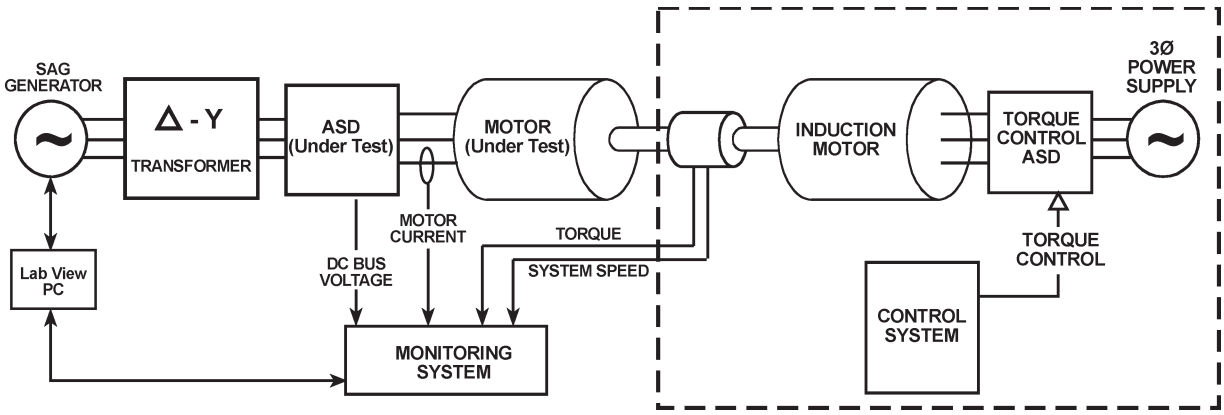

Fig. 10. Experimental test-equipment configuration.

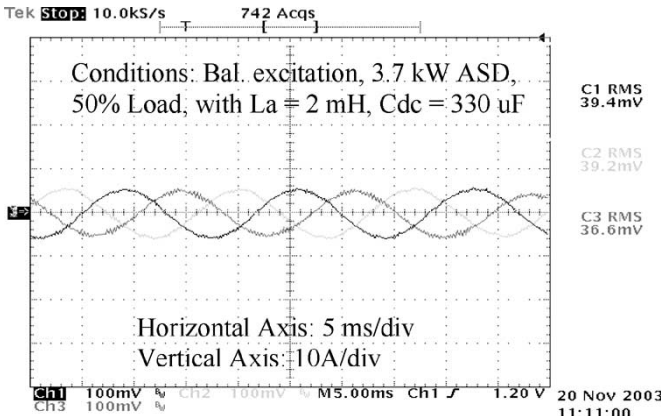

Fig. 11. Measured stator-current waveforms during balanced excitation at 460-V input voltage (50% load).

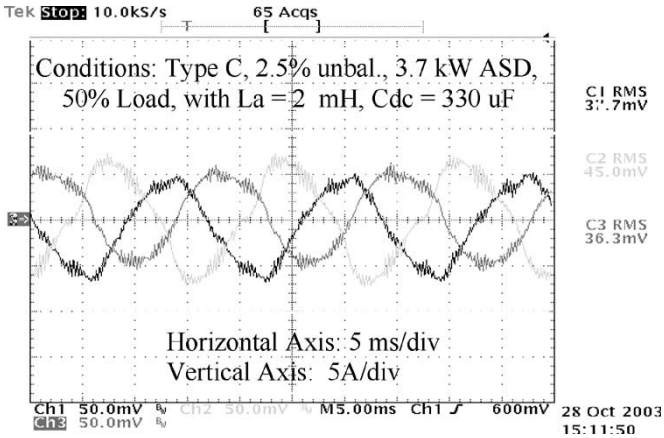

Fig. 12. Measured stator-current waveforms during type-C sag with 2.5% voltage unbalance (50% load).

principally at the second harmonic of the input line frequency (i.e., 120 Hz).

In addition, this analysis shows why harmonic-current components at the sum and difference frequencies of $[(\omega_0 + 2\omega_{\rm i})$ and $(\omega_0 - 2\omega_{\rm i})]$ appear in the machine stator currents as a result of the input line unbalance conditions.

The availability of these closed-form expressions makes it possible to rapidly calculate the impact of varying values of input line-voltage sag or unbalance on the operating characteristics of an induction machine excited by a general-purpose (volts per hertz) ASD. It is important to emphasize that this closed-form analysis has been carried out for finite values of input line inductances and dc bus capacitance, providing a valuable contribution beyond work previously reported in the technical literature. In particular, this analytical tool provides a useful tool to aid the development of effective sag mitigation techniques.

TABLE I
PULSATING-TORQUE COMPARISON BETWEEN CLOSED-FORM ANALYSIS, SIMULATION, AND EXPERIMENTAL RESULTS

Conditions: Type C, 2.5% Unb. 50% load	*Peak-to-Peak Pulsating Torque (Nm)*	*Percentage of Average Torque*
Closed-Form	3.38	33.8%
Simulation	3.36	33.6%
Experiment	3.21	32.1%

Conditions: 3.7-kW ASD at 50% load with a type-C Sag at 2.5% unbalance

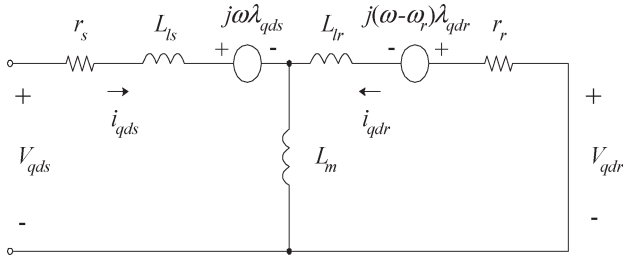

Fig. 13. Complex dq equivalent circuit of a three-phase induction machine in a rotating reference frame (ω).

APPENDIX
CLOSED-FORM DERIVATION

In order to calculate the phase currents for unbalanced excitation, the three phase voltages can be transformed into a complex dq voltage space vector in a rotating reference frame and then applied to the appropriate complex dq equivalent circuit for the induction machine shown in Fig. 13, [15].

The definitions of the complex variables include [15] the following:

v_{qds} complex stator voltage;
v_{qdr} complex rotor voltage;
$r_{\rm s}$ stator resistance;

λ_{qds} stator flux linkage;
$L_{\rm s}$ total stator inductance;
$L_{\rm r}$ total rotor inductance;
$L_{\rm m}$ magnetizing inductance;
i_{qds} complex stator current;
i_{qdr} complex rotor current;
$r_{\rm r}$ rotor resistance;
λ_{qdr} rotor flux linkage;
$L_{\rm ls}$ stator leakage inductance;
$L_{\rm lr}$ rotor leakage inductance.

The induction-machine inductances and flux linkages are defined as

$$L_{\rm s} = L_{\rm ls} + L_{\rm m} \tag{A1}$$

$$L_{\rm r} = L_{\rm lr} + L_{\rm m} \tag{A2}$$

$$\lambda_{qds} = L_{\rm s} \cdot i_{qds} + L_{\rm m} \cdot i_{qdr} \tag{A3}$$

$$\lambda_{qdr} = L_{\rm s} \cdot i_{qdr} + L_{\rm m} \cdot i_{qds}. \tag{A4}$$

The following differential equations govern the behavior of the electrical variables in Fig. 13:

$$v_{qds} = i_{qds} \cdot r_{\rm s} + (p + j\omega) \cdot \lambda_{qds} \tag{A5}$$

$$v_{qdr} = i_{qdr} \cdot r_{\rm r} + [p + j(\omega - \omega_{\rm r})] \cdot \lambda_{qdr} \tag{A6}$$

where p represents the differentiation operator (d/dt), ω is the angular velocity of an arbitrary reference frame, and $\omega_{\rm r}$ is the rotor angular velocity.

For this problem, it is convenient to carry out the analysis in the reference frame that is synchronous with the inverter output frequency so that $\omega = \omega_0$ in (A5) and (A6) above. Combining this substitution with (A1)–(A4) leads to

$$V^e_{qds} = [r_{\rm s} + L_{\rm s} \cdot (p + j\omega_0)] \cdot i^e_{qds} + L_{\rm m} \cdot (p + j\omega_0) \cdot i^e_{qdr} \tag{A7}$$

$$V^e_{qdr} = [r_{\rm r} + L_{\rm r} \cdot (p + j(\omega_0 - \omega_{\rm r}))] \cdot i^e_{qdr} + L_{\rm m} \cdot [p + j(\omega_0 - \omega_{\rm r})] \cdot i^e_{qds} \tag{A8}$$

where the superscript e indicates that the variables are expressed in the synchronous reference frame.

Superposition can be used to determine the machine response to the three frequency terms in the unbalanced phase voltages (10) on a term-by-term basis. Consider first the phase voltages associated with the ω_0 term

$$V_{a0}[\omega_0 t] = \frac{1}{2} \cdot V_{\rm dc} \cdot B_1 \cdot \sin(\omega_0 t) \tag{A9}$$

$$V_{bo}[\omega_0 t] = \frac{1}{2} \cdot V_{\rm dc} \cdot B_1 \cdot \sin(\omega_0 t - 120^\circ) \tag{A10}$$

$$V_{c0}[\omega_0 t] = \frac{1}{2} \cdot V_{\rm dc} \cdot B_1 \cdot \sin(\omega_0 t + 120^\circ). \tag{A11}$$

These three phase voltages can be transformed into a dq complex vector in the synchronous frame using

$$v^e_{qds} = \frac{2}{3} \cdot (V_{a0} + a \cdot V_{b0} + a^2 \cdot V_{c0}) \cdot e^{-j\omega_0 t} \tag{A12}$$

where

$$a = e^{j\frac{2}{3}\pi} \tag{A13}$$

$$1 + a + a^2 = 0. \tag{A14}$$

Defining $K_0 = 1/2 \cdot V_{\rm dc} \cdot B_1$ and applying (A12)–(A14) to (A9)–(A11) leads to

$$v^e_{qds}[\omega_0 t] = K_0. \tag{A15}$$

Similarly, the three phase voltages associated with the $2\omega_{\rm i} + \omega_0$ and $2\omega_{\rm i} - \omega_0$ terms in (10) can be transformed into synchronous-frame complex voltage vectors as

$$v^e_{qds}[(2\omega_{\rm i} + \omega_0)t] = K_1 \cdot e^{j\theta_2} \cdot e^{j2\omega_{\rm i} t} \tag{A16}$$

$$v^e_{qds}[-(2\omega_{\rm i} - \omega_0)t] = K_1 \cdot e^{-j\theta_2} \cdot e^{-j2\omega_{\rm i} t} \tag{A17}$$

where $K_1 = 1/4 \cdot V_{\rm dc} \cdot B_1$, so the complete expression for v^e_{qds} is

$$v^e_{qds} = K_0 + K_1 \cdot e^{j\theta 2} \cdot e^{j2\omega_{\rm i} t} + K_1 \cdot e^{-j\theta 2} \cdot e^{-j2\omega_{\rm i} t}. \tag{A18}$$

The induction-machine equations (A7) and (A8) can then be used to solve for the resulting stator and rotor complex current variables i^e_{qds} and i^e_{qdr}, respectively. For a squirrel-cage induction machine, the rotor terminal voltage is zero ($v^e_{qdr} = 0$). For simplicity, it will be assumed that $\theta_2 = 0$.

Applying superposition, the stator and rotor currents will have the following forms:

$$i^e_{qds} = I_{\rm s0} + I_{\rm s1} e^{j2\omega_{\rm i} t} + I_{\rm s2} e^{-j2\omega_{\rm i} t} \tag{A19}$$

$$i^e_{qdr} = I_{\rm r0} + I_{\rm r1} e^{j2\omega_{\rm i} t} + I_{\rm r2} e^{-j2\omega_{\rm i} t} \tag{A20}$$

where the coefficients can be evaluated as

$$I_{\rm s0} = b_0 \cdot K_0 \quad I_{\rm r0} = b_0 \cdot c_o \cdot K_0 \tag{A21}$$

$$b_0 = \left[r_{\rm s} + j\omega_0 L_{\rm s} + \frac{L^2_{\rm m} \omega_0 (\omega_0 - \omega_{\rm r})}{r_{\rm r} + L_{\rm r} \cdot j(\omega_0 - \omega_{\rm r})} \right]^{-1} \tag{A22}$$

$$c_o = \frac{-jL_{\rm m}(\omega_0 - \omega_{\rm r})}{r_{\rm r} + jL_{\rm r}(\omega_0 - \omega_{\rm r})} \tag{A23}$$

$$I_{\rm s1} = b_1 \cdot K_1 \quad I_{\rm r1} = b_1 \cdot c_1 \cdot K_1 \tag{A24}$$

$$b_1 = \left[r_{\rm s} + L_{\rm s} \cdot j(2\omega_{\rm i} + \omega_0) + \frac{L^2_{\rm m}(2\omega_{\rm i} + \omega_0)(2\omega_{\rm i} + \omega_0 - \omega_{\rm r})}{r_{\rm r} + L_{\rm r} \cdot j(2\omega_i + \omega_0 - \omega_{\rm r})} \right]^{-1} \tag{A25}$$

$$c_1 = \frac{-L_{\rm m} \cdot j(2\omega_{\rm i} + \omega_0 - \omega_{\rm r})}{r_{\rm r} + L_{\rm r} \cdot j(2\omega_i + \omega_0 - \omega_{\rm r})} \tag{A26}$$

$$I_{\rm s2} = b_2 \cdot K_1 \quad I_{\rm r2} = b_2 \cdot c_2 \cdot K_1 \tag{A27}$$

$$b_2 = \left[r_{\rm s} + L_{\rm s} j(-2\omega_{\rm i} + \omega_0) + \frac{L^2_{\rm m}(-2\omega_{\rm i} + \omega_0)(-2\omega_{\rm i} + \omega_0 - \omega_{\rm r})}{r_{\rm r} + L_{\rm r} j(-2\omega_{\rm i} + \omega_0 - \omega_{\rm r})} \right]^{-1} \tag{A28}$$

$$c_2 = \frac{-L_{\rm m} \cdot j(-2\omega_{\rm i} + \omega_0 - \omega_{\rm r})}{r_{\rm r} + L_{\rm r} \cdot j(-2\omega_i + \omega_0 - \omega_{\rm r})}. \tag{A29}$$

The electromagnetic torque impressed on the shaft of the induction machine can be expressed as [15]

$$T_{\rm e} = \frac{3}{2} \times \frac{P}{2} \times L_{\rm m} \times I_m \left[i^{e}_{qd\rm s} \times i^{\rm e^*}_{qd\rm r} \right] \qquad \text{(A30)}$$

where P is the number of poles and the last term represents the imaginary part of the product of the complex stator current and the complex conjugate of the rotor current. The expressions for the complex stator and rotor currents in (A19) and (A20) can be used to develop an expression for the product in (A30) as follows:

$$\begin{aligned} i^{e}_{qd\rm s} \times i^{\rm e^*}_{qd\rm r} &= I_{\rm s0} \cdot I_{\rm r0} + I_{\rm s1} \cdot I_{\rm r1} + I_{\rm s2} \cdot I_{\rm r2} \\ &\quad + (I_{\rm s0} \cdot I_{\rm r1} + I_{\rm s2} \cdot I_{\rm r0} + I_{\rm s2} \cdot I_{\rm r1}) \cdot e^{-j2\omega_{\rm i} t} \\ &\quad + (I_{\rm s0} \cdot I_{\rm r2} + I_{\rm s1} \cdot I_{\rm r0}) \cdot e^{j2\omega_{\rm i} t} + I_{\rm s1} \cdot I_{\rm r2} \cdot e^{j4\omega_{\rm i} t}. \end{aligned} \qquad \text{(A31)}$$

Evaluating (A30) with (A31) leads to the following expression for the instantaneous torque

$$T_{\rm e} = T_{\rm e0} + T_{\rm e2} \cos(2\omega_{\rm i} t + \phi_2) + T_{\rm e4} \cos(4\omega_{\rm i} t + \phi_4). \qquad \text{(A32)}$$

This expression shows that, during unbalanced input-voltage excitation conditions, the torque consists of three terms including an average torque, a component at twice the line excitation frequency, and a component at four times the line frequency. This is an approximate expression since it only includes the effects of the second harmonic of the line frequency in the dc bus voltage, as shown in (7).

The parameters of the 3.7-kW 460-$V_{\rm rms}$ induction machine used in evaluating these closed-form expressions as well as for carrying out the dynamic simulations are

$$\begin{aligned} &r_{\rm s} = 1.58\ \Omega \qquad r_{\rm r} = 1.23\ \Omega \qquad L_{\rm ls} = 17.4\ \text{mH} \\ &L_{\rm lr} = 23.3\ \text{mH} \quad L_{\rm m} = 258\ \text{mH} \quad J = 0.0252\ \text{kg} \cdot \text{m}^2. \end{aligned} \qquad \text{(A33)}$$

REFERENCES

[1] M. H. J. Bollen, *Understanding Power Quality Problems—Voltages and Interruptions*. New York: IEEE Press, 1999.

[2] D. O. Koval, R. A. Bocancea, K. Yao, and M. B. Hughes, "Canadian national power quality survey: Frequency and duration of voltage sags and surges at industrial sites," *IEEE Trans. Ind. Appl.*, vol. 34, no. 5, pp. 904–910, Sep./Oct. 1998.

[3] C. J. Melhorn and M. F. McGranaghan, "Interpretation and analysis of power quality measurements," *IEEE Trans. Ind. Appl.*, vol. 31, no. 6, pp. 1363–1370, Nov./Dec. 1995.

[4] *Electric Power Systems and Equipment—Voltage Ratings (60 Hertz)*. Available: ANSI Standard Publication no. ANSI C84.1-1989/1995/2001.

[5] J. P. G. de Abreu and A. E. Emanuel, "Induction motor thermal aging caused by voltage distortion and imbalance: Loss of useful life and its estimated cost," *IEEE Trans. Ind. Appl.*, vol. 38, no. 1, pp. 12–20, Jan./Feb. 2000.

[6] S. M. Abdulrahman, J. Gordon, and I. R. Smith, "Fast calculation of harmonic torque pulsations in a VSI/induction motor drive," *IEEE Trans. Ind. Electron.*, vol. 40, no. 6, pp. 561–569, Dec. 1993.

[7] T. A. Lipo, P. C. Krause, and H. E. Jordan, "Harmonic torque and speed pulsations in a rectifier-inverter induction motor drive," *IEEE Trans. Power App. Syst.*, vol. PAS-88, no. 5, pp. 579–587, May 1969.

[8] W. D. Frank, "Torque ripple considerations on large (mill) drives in the cement industry," in *Proc. IEEE XXXVII Cement Ind. Tech. Conf.*, Jun. 1995, pp. 411–432.

[9] J. J. Spangler, "A low cost, simple torque ripple reduction technique for three phase inductor motors," in *Proc. IEEE APEC*, Mar. 2002, vol. 2, pp. 759–763.

[10] A. Nystrom, J. Hylander, and K. Thorborg, "Harmonic currents and torque pulsations with pulse width modulation methods in AC motor drives," in *Proc. 3rd Int. Conf. Power Electron. Adjustable-Speed Drives*, Jul. 1988, pp. 378–381.

[11] E. Muljadi, T. Batan, D. Yildirim, and C. P. Butterfield, "Understanding the unbalanced-voltage problem in wind turbine generation," in *Conf. Rec. IEEE-IAS*, Oct. 1999, vol. 2, pp. 1359–1365.

[12] S. Williamson and S. Smith, "Pulsating torque and losses in multiphase induction machines," *IEEE Trans. Ind. Appl.*, vol. 39, no. 4, pp. 986–993, Jul./Aug. 2003.

[13] K. Lee, G. Venkataramanan, and T. M. Jahns, "Design-oriented analysis of dc-bus dynamics in adjustable speed drives under input voltage unbalance and sag conditions," in *Proc. IEEE PESC*, Aachen, Germany, Jun. 2004, pp. 1675–1681.

[14] L. Moran, P. D. Ziogas, and G. Joos, "Design aspects of synchronous PWM rectifier-inverter systems under unbalanced input voltage conditions," *IEEE Trans. Ind. Appl.*, vol. 28, no. 6, pp. 1286–1293, Nov./Dec. 1992.

[15] D. W. Novotny and T. A. Lipo, *Vector Control and Dynamics of ac Drives*. New York: Oxford Univ. Press, 1998.

Kevin Lee (M'90–SM'05) received the B.E.E. degree from TsingHua University, Beijing, China, in 1986, and the M.S.E.E. degree from Rensselaer Polytechnic Institute, Troy, NY, in 1990. He is currently working toward the Ph.D. degree in electrical engineering in the Wisconsin Electric Machines and Power Electronics Consortium (WEMPEC) group, at the University of Wisconsin, Madison.

Before joining Eaton Electrical, Milwaukee, WI, in 1998, he was previously with Hevi-Duty Electric, a Unit of General Signal (now SPX Corporation) between 1990–1998 and was the Engineering Manager for airport lighting products. Currently, he is a Principal Engineer at the Innovation Center, Eaton Corporation. His design and research interests include power quality, motor drives, uninterruptible power systems (UPSs), and power electronics with applied modern control theories. He is the holder of one U.S. patent and has three others pending.

Mr. Lee is a Registered Professional Engineer in the State of Wisconsin.

Thomas M. Jahns (S'73–M'79–SM'91–F'93) received the S.B. and S.M., and Ph.D. degrees in electrical engineering from the Massachusetts Institute of Technology, Cambridge, in 1974 and 1978, respectively.

From 1996 to 1998, he conducted a research sabbatical at the Massachusetts Institute of Technology, where he directed research activities in the area of advanced automotive electrical systems and accessories as Codirector of an industry-sponsored automotive consortium. Prior to joining the University of Wisconsin (UW), Madison, he was with GE Corporate Research and Development, Schenectady, NY, for 15 years, where he pursued new power electronics and motor drive technology in a variety of research and management positions. In 1998, he joined the Department of Electrical and Computer Engineering, UW, Madison, as a Professor. Currently, he is the Associate Director of the Wisconsin Electric Machines and Power Electronics Consortium (WEMPEC), at UW, Madison. His research interests include permanent-magnet synchronous machines for a variety of applications ranging from high-performance machine tools to low-cost appliance drives.

Dr. Jahns was awarded the William E. Newell Award by the IEEE Power Electronics Society (PELS) in 1999. He was recognized as a Distinguished Lecturer by the IEEE Industry Applications Society (IAS) in 1994–1995 and by IEEE-PELS in 1998–1999. He has served as President of PELS (1995–1996) and as a member of the IAS Executive Board from 1992 to 2001.

William E. Berkopec received the B.S. degree in electrical engineering from the University of Wisconsin, Madison, in 1969.

He has over 36 years of experience in design and development engineering, which has involved dc drives, adjustable-frequency drives, active rectifiers, and reduced-voltage induction-motor starters. Of these 36 years, a total of 33 years have been with the Eaton Corporation. He worked for their Drives Division in Kenosha, WI, and Oldsmar, FL, and their Corporate Research and Development Division in Milwaukee, WI. Presently, he is an Associate of the Eaton Electrical Industrial Control Division, Milwaukee, WI. He is listed as a coinventor on four U.S. patents.

Thomas A. Lipo (M'64–SM'71–F'87–LF'04) was born in Milwaukee, WI. He received the B.E.E. and M.S.E.E. degrees from Marquette University, Milwaukee, WI, in 1962 and 1964, respectively, and the Ph.D. degree in electrical engineering from the University of Wisconsin, Madison, in 1968.

From 1969 to 1979, he was an Electrical Engineer in the Power Electronics Laboratory of Cooperate Research and Development of the General Electric Company, Schenectady, NY. He became a Professor of Electrical Engineering at Purdue University, West Lafayette, IN, in 1979, and in 1981, he joined the University of Wisconsin, Madison, in the same capacity, where he is presently the W. W. Grainger Professor for Power Electronics and Electrical Machines, Codirector of the Wisconsin Electric Machines and Power Electronics Consortium, and Director of the Wisconsin Power Electronics Research Center. He has authored more than 400 published technical papers and is the holder of 32 U.S. patents.

Dr. Lipo received the 1986 Outstanding Achievement Award from the IEEE Industry Applications Society (IAS), the 1990 William E. Newell Award of the IEEE Power Electronics Society, and the 1995 Nicola Tesla IEEE Field Award from the IEEE Power Engineering Society for his work. He has served the IEEE in various capacities for three IEEE Societies, including as President of the IAS. He is a Fellow of the Institution of Electrical Engineers, U.K., and the Royal Academy of Engineering (Great Britain), and a member of the Institute of Electrical Engineers of Japan. He has received 21 IEEE Prize Paper Awards from three different IEEE Societies including Best Paper Awards for publication in the IEEE TRANSACTIONS in the years 1984, 1994, and 1999.